ELSEVIER

Contents lists available at ScienceDirect

# Journal of Inorganic Biochemistry

journal homepage: www.elsevier.com/locate/jinorgbio





# Oxygen-selective regulation of cyclic di-GMP synthesis by a globin coupled sensor with a shortened linking domain modulates *Shewanella* sp. ANA-3 biofilm

Ariel Schuelke-Sanchez<sup>a</sup>, Neela H. Yennawar<sup>b</sup>, Emily E. Weinert<sup>a,c,\*</sup>

- <sup>a</sup> Department of Biochemistry and Molecular Biology, Pennsylvania State University, University Park, PA 16802, USA
- b The Huck Institutes of the Life Sciences, Pennsylvania State University, University Park, PA 16802, USA
- <sup>c</sup> Department of Chemistry, Pennsylvania State University, University Park, PA 16802, USA

#### ARTICLE INFO

# Keywords: Heme Oxygen sensing Globin Diguanylate cyclase Biofilm

#### ABSTRACT

Bacteria utilize heme proteins, such as globin coupled sensors (GCSs), to sense and respond to oxygen levels. GCSs are predicted in almost 2000 bacterial species and consist of a globin domain linked by a central domain to a variety of output domains, including diguanylate cyclase domains that synthesize *c*-di-GMP, a major regulator of biofilm formation. To investigate the effects of middle domain length and heme edge residues on GCS diguanylate cyclase activity and cellular function, a putative diguanylate cyclase-containing GCS from *Shewanella* sp. ANA-3 (*SA*3GCS) was characterized. Binding of O<sub>2</sub> to the heme resulted in activation of diguanylate cyclase activity, while NO and CO binding had minimal effects on catalysis, demonstrating that *SA*3GCS exhibits greater ligand selectivity for cyclase activation than many other diguanylate cyclase-containing GCSs. Small angle X-ray scattering analysis of dimeric *SA*3GCS identified movement of the cyclase domains away from each other, while maintaining the globin dimer interface, as a potential mechanism for regulating cyclase activity. Comparison of the *Shewanella* ANA-3 wild type and *SA*3GCS deletion (Δ*SA*3GCS) strains identified changes in biofilm formation, demonstrating that *SA*3GCS diguanylate cyclase activity modulates *Shewanella* phenotypes.

# 1. Introduction

The Shewanella species are a diverse group of facultative anaerobic bacteria that are widely distributed in aquatic environments. The greatest asset of many Shewanella species is the ability to utilize a diverse set of electron acceptors that include toxic elements and insoluble metals [4]. The remarkably diverse respiratory versatility allows for survival in an array of environmental conditions. As such, these bacteria have been shown to facilitate bioremediation and in bioengineering applications [5,6]. In addition, Shewanella species typically form robust biofilm in diverse environments, such as on green algae [7] and mineral surfaces [8]. Biofilms are three dimensional bacterial communities that form on surfaces and provide protection from predation and environmental stressors, and, in the case of pathogenic bacteria, can be required for successful infection [9].

Bacterial biofilm formation is modulated by extracellular signals [10], including oxygen  $(O_2)$ . As Shewanella species can respire both aerobically and anaerobically, the bacteria must be able to change the

terminal oxidant used in metabolism based on their environment [11]. In addition to *Shewanella* altering metabolism in response to  $O_2$  levels, many other bacteria have been shown to alter biofilm formation (surface attached bacterial communities), motility, and virulence, suggesting that  $O_2$  levels are monitored by many bacterial species [12–16].

A class of widely distributed heme proteins, termed globin coupled sensors, may be serving as environmental  $O_2$  sensors within bacteria and allowing for response to changing gas levels [15,17–19]. Globin coupled sensor (GCS) proteins consist of a N-terminal globin domain that is linked to a C-terminal output domain by a variable middle domain and activity of the output domain is modulated by diatomic gaseous ligands. GCSs contain many types of output domains [20–22], such as diguanylate cyclase domains [15–17,23,24], which are responsible for synthesizing 3′,5′-cyclic dimeric guanosine monophosphate (c-di-GMP). C-di-GMP is a ubiquitous bacterial secondary messenger that plays a regulatory role in several cellular pathways and processes, such as biofilm formation [10,24]. Low levels of c-di-GMP have been shown to regulate the motile-sessile transition of bacteria and typically result in increased

<sup>\*</sup> Corresponding author at: Department of Biochemistry and Molecular Biology, Pennsylvania State University, University Park, PA 16802, USA. *E-mail address:* emily.weinert@psu.edu (E.E. Weinert).

motility. Conversely, high levels of c-di-GMP production have shown to promote surface attachment and biofilm formation [25].

Diguanylate cyclase-containing GCS proteins have been identified across different bacterial genomes, suggesting widespread importance in regulating O2-dependent bacterial phenotypes. While the sensor globin and diguanylate cyclase domains of GCS proteins typically exhibit sequence homology, the middle domains of predicted GCS proteins vary in length (from  $\sim$ 13–140 amino acids). To date, the majority of work on diguanylate cyclase (DGC)-containing GCS proteins has focused on those with long (~130-140 amino acid) middle domains, such as the GCS proteins from Bordetella pertussis (BpeGReg; causative agent of whooping cough), Escherichia coli (EcDosC), and Pectobacterium carotovorum (PccGCS; soft rot plant pathogen) [17], while only one diguanylate cyclase-containing GCS with a shorter middle domain (~40 amino acids) has been characterized (HemDGC from Desulfotalea psychrophila) [16]. Characterization of the ligand-dependent enzyme activity, conformation, and physiological role of a globin-coupled sensor from Shewanella sp. strain ANA-3 (SA3GCS), which is predicted to contain an N-terminal sensor globin connected by a ~ 40 amino acid middle domain to a C-terminal diguanylate cyclase domain, has provided further insights into the role shortened middle domain on GCS signaling.

#### 2. Materials and methods

#### 2.1. SA3GCS protein expression and purification

The *Escherichia coli* codon-optimized gene encoding SANA3GCS was inserted into a previously created pHis-maltose binding protein (MBP) vector [26], containing a tobacco etch virus (TEV) protease cleavage site and an MBP tag, using polymerase incomplete primer extension (PIPE) cloning (Table S1). Plasmid pHis-MBP-Sana3GCS was transformed into *E. coli* strain Tuner (DE3) pLysS (Lucigen). The cells were overexpressed in a yeast extract expression media [27] containing ampicillin (100  $\mu g$  mL $^{-1}$ ) and chloramphenicol (30  $\mu g$  mL $^{-1}$ ) at 37 °C, 225 rpm to an OD $_{600} \sim 0.3$ . The temperature was dropped to 18 °C and enough  $\delta$ -aminolevunlinic acid was added to reach a final concentration of 500  $\mu M$ . Protein expression was induced when the OD $_{600}$  reached 0.7 by the addition of 100  $\mu M$  IPTG and the cultures were incubated at 18 °C with shaking overnight. Cells were harvested by centrifugation (3500 xg, 4 °C, 20 min) and stored at -80 °C.

To purify MBP tagged SA3GCS, the cell pellets were suspended in a buffer consisting of 50 mM Tris at pH 8.0, 300 mM NaCl, 300 mM imidazole, and 5% glycerol ( $\nu/\nu$ ). Cells were lysed by sonication in the presence of the protease inhibitors, benzamidine HCl and Pefabloc at 60% amplitude for 30 s on/off for a total of 12 min. The lysate was clarified by centrifugation (Beckman Optima L-90× ultracentrifuge) at 130,000 x g, 4 °C for 1 h. The supernatant was applied to a preequilibrated HisPur Ni column (Fisher Scientific). SA3GCS eluted in a buffer consisting of 50 mM Tris at pH 8.0, 300 mM NaCl, and 250 mM imidazole at a flow rate of 1.0 mL min $^{-1}$ .

The cleavage of MBP is necessary to obtain SA3GCS with high enzymatic activity. S219V TEV protease (expression/purification conditions below) was added to MBP tagged SA3GCS in a OD280 ratio of 5:100 with sufficient dithiothreitol and ethylenediaminetetraacetic acid to reach final concentrations of 1 mM and 0.5 mM, respectively. The mixture was dialyzed for three hours, twice, against a buffer consisting of 50 mM Tris at pH 8.0, 300 mM NaCl, and 5% glycerol (v/v) at 4 °C. Enough imidazole was added to the dialyzed protein to reach a concentration of 20 mM and the protein was loaded onto a HisPur Ni-NTA column equilibrated with a buffer consisting of 50 mM Tris, 300 mM NaCl, 20 mM imidazole, and 5% glycerol (v/v) at pH 8.0. Following protein loading, the column was washed with the same buffer described above. The protein was collected and concentrated via ultrafiltration (YM-10, 10 kDa MWCO filter, Milipore). Purified SA3GCS was desalted and further purified by size exclusion chromatography (SEC) using a S200 gel filtration column (GE Healthcare) equilibrated with a buffer

consisting of 50 mM Tris at pH 8.0, 50 mM NaCl, 1 mM DTT, and 5% glycerol (v/v; Buffer A) at a flow rate of 1.0 mL min<sup>-1</sup>. Fractions containing *SA*3GCS were collected and concentrated via ultrafiltration, flash frozen, and stored at  $-80\,^{\circ}$ C until use. Protein purity was assessed by sodium dodecyl sulfate-polyacrylamide gel electrophoreses (SDS-PAGE) (Fig. S1), and concentrations were determined using the Bradford Microassay (Bio-Rad Laboratories).

#### 2.2. TEV protease expression and purification

S219V TEV protease vector pRk793 was a gift from Prof. Michael Marletta (UC- Berkley). The plasmid was transformed into *E. coli* BL21 DE3 cells and cells grown in LB media containing 100  $\mu g$  mL $^{-1}$  ampicillin and 30  $\mu g$  mL $^{-1}$  chloramphenicol at 37 °C with shaking to an OD $_{600}\sim0.6$ . TEV expression was induced with 1 mM IPTG and then cells were incubated with shaking at 37 °C for four hours. The cells were harvested after centrifugation (3500 xg, 4 °C, 20 min) and stored at -80 °C.

To purify TEV protease, the cell pellets were resuspended in buffer consisting of 20 mM NaPi and 300 mM NaCl at pH 7.5. Cells were lysed by sonication (QSonica) in the presence of the protease inhibitors benzamidine HCl (Dot Scientific) and Pefablock (Sigma-Aldrich) at 60% amplitude for 30 s on/off for a total of 6 min on. The lysate was clarified by centrifugation (Beckman Optima L-90  $\times$  ultracentrifuge) at 130,000 x g, 4  $^{\circ}$ C for 1 h. The supernatant was applied to a HiTrap HP 5 mL column (GE Healthcare) equilibrated with a buffer, which consisted of 20 mM NaPi and 300 mM NaCl at pH 7.5, using a NGC Chromatography system (Biorad). The loaded column was washed with a gradient from 0 mM imidazole to 40 mM imidazole over 2 column volumes and eluted at 200 mM imidazole. The purified protein was dialyzed against a buffer consisting of 20 mM NaPi and 300 mM NaCl at pH 7.5 for three hours, two times. Purified protein was collected, concentrated, flash frozen, and stored at  $-80\,^{\circ}$ C for future use.

# 2.3. UV-visible absorption spectroscopy

UV–visible absorption spectroscopy spectra were acquired from 800 to 200 nm using an Agilent Cary 100 spectrophotometer. Spectra were recorded in a 1 cm path length quartz cuvette. Preparation of complexes were carried out as previously described. [28,29] Briefly, SA3GCS was transferred into the anaerobic chamber (Coy) and incubated with sodium dithionite (Millipore Sigma) for 30 min. The mixture was then desalted using a PD-10 column (GE Healthcare) that was equilibrated with Buffer A and checked using the spectrophotometer for the fully reduced Fe(II) ligation state. For the Fe(II)-NO sample, 5  $\mu$ L of 10 mM DEA-NONOate (Cayman Chemical) dissolved in anaerobic 0.1 M NaOH was added to the protein. For the Fe(II)-O2 state, reduced SA3GCS was removed from the anaerobic chamber and mixed with aerobic or O2 saturated Buffer A. The CO complex was generated by introducing CO gas into the headspace of an anaerobic cuvette (Starna Cells) containing Fe(II) SA3GCS.

# 2.4. Enzyme kinetics

Enzyme kinetic assays were performed to determine the diguanylate cyclase activity of SA3GCS with the EnzChek pyrophosphate kit (Life Technologies) [30]. Prior to kinetic measurements, SA3GCS and EcDosP [31], which was expressed and purified as previously described, were reduced and various SA3GCS complexes were formed as previously described. [28,29] The ligation/oxidation state of the heme was determined by UV-visible spectroscopy before each enzyme assay. Enzyme kinetics with all Fe(II), Fe(II) – CO, and Fe(II) – NO ligation states were measured in an anaerobic chamber (Coy Laboratories). The EnzCheck pyrophosphate kit instructions were followed with the exception that SA3GCS and a phosphodiesterase, EcDosP, were added and the reactions were initiated with varying concentrations of GTP (Sigma). Briefly,

inorganic pyrophosphate (PPi) is converted to inorganic phosphate (Pi) via inorganic pyrophosphatase (IP). Pi is used to enzymatically convert 2-amino-6-mercapto-7-methylpurine ribonucleoside (MESG) to ribose 1-phosphate and 2 -amino-6-mercapto-7-methylpurine. The enzymatic conversion of MESG results in a shift in its absorbance maximum from 330 nm to 360 nm.

The assays were performed in triplicate in 96 well plates (Corning) containing 4 protein concentrations (0.05–0.4  $\mu M)$  and 6 GTP concentrations (0–500 mM). EcDosP was included at a 3-M excess to eliminate inhibition of cyclase activity by the produced c-di-GMP. The entire plate assay (including triplicates) was monitored at 360 nm every 30 s for 180 min using an Epoch2 plate reader and Gen5 software (Biotek). The assays were repeated at least twice with different protein from different expressions/purifications to account for protein batch variability. Analyses to determine enzymatic rates were performed using Igor Pro (Wavemetrics).

#### 2.5. O<sub>2</sub> dissociation measurements

 $O_2$  dissociation measurements were performed as previously described [17,27,28], with the following modifications. SA3GCS Fe(II)- $O_2$  ligation state was formed as described above. A 10 mM sodium dithionite trap was prepared in anaerobic Buffer A in an anaerobic chamber (Coy Labs). CO was not used as part of the trap. The dissociation of  $O_2$  from the heme was monitored using an SX20 stopped flow equipped with diode array detector and fit globally using Pro-KII (Applied Photophysics). Additional fitting analysis of raw data was performed using Igor Pro (Wavemetrics) (Fig. S2). Amplitudes of each fitted rate constant were calculated by fitting the data using a biexponential equation in Igor Pro. Amplitudes of each phase were used to calculate the percentage of each rate constant by dividing the amplitude of  $k_I$  or  $k_2$  by the sum of the amplitudes and multiplying by 100.

#### 2.6. Size Exclusion Chromatography (SEC)

SA3GCS oligomers were detected via size exclusion chromatography using an Agilent 1200 infinity system with a Sepax SEC-300 (7.8 mm  $\times$  300 mm, 300 Å) and diode array detector (simultaneous detection at 214, 280, 416, and 431 nm), as previously described. [17] SA3GCS and MBP-SA3GCS were reduced in an anaerobic chamber and then allowed to bind  $O_2$  following mixing with aerobic buffer. A UV–visible spectrum was collected to determine the ligation state of the heme. The mobile phase for all experiments consisted of a 150 mM NaPi buffer at pH 8.0. Spectra were collected for each peak during the SEC run to confirm that the heme remained in the  $Fe^{II}$ – $O_2$  ligation state. Globular proteins (Sigma-Aldrich) consisting of thyroglobulin (640 kDa),  $\gamma$ -globulin (155 kDa), ovalbumin (47 kDa), and ribonuclease A (13.7 kDa) were used as molecular weight standards for calibration curves.

#### 2.7. Circular Dichroism (CD) spectroscopy

The secondary structure of SA3GCS at different ligation states were assessed using circular dichroism (CD) spectroscopy. Triplicate samples of 0.1 mg/mL Fe(II) and Fe(II) –  $O_2$  MBP-SA3GCS were prepared as described above in 10 mM potassium phosphate (KPi) pH 8.0 and loaded into a 1 mm path length quartz cuvette. For anaerobic CD measurement, the cuvette was sealed in the glove box. The UV CD spectra were collected with a Jasco J-1500 CD spectrometer at room temperature setting, bandwidth of 1 nm, response time of 1 s, standard sensitivity, wavelength scan range from 260 to 185 nm with a scan rate of 50 nm/min and 0.5 nm data interval (Fig. S3) and a three-scan accumulation (averaged at the end). The spectra for the samples were normalized by subtracting a spectrum of the buffer alone under the same conditions. Data analysis and the determination of the standard error were done using Microsoft Excel. The secondary structure was estimated using the BestSel program [32].

#### 2.8. Dynamic Light Scattering (DLS)

Purified Fe(II)– $O_2$  MBP-SA3GCS protein was checked for its quality and size distribution with a DLS run prior to the small-angle X-ray scattering (SAXS) experiment. DLS was performed on 0.5 mg/mL Fe(II)– $O_2$  MBP-SA3GCS in Buffer A using a Viscotek802 DLS instrument at 293 K. The DLS data were processed by the OmniSIZE 3.0 software to get an estimate of the hydrodynamic radii and sizes of the sample population. The estimated Rh of the two major peaks were 87 and 707 Å and the polydispersity of peaks was 0.29 and 0.288, respectively (Fig. S4). The hydrodynamic radii suggested that at room temperature a mixed population of dimers, higher order oligomeric states and larger aggregates (>100 nm) appear in the size distribution intensity existed in solution. This necessitated the use of inline SEC-SAXS to separate and study the dimers individually.

#### 2.9. SAXS measurement and modeling

Synchrotron SEC-SAXS data of Fe(II)-O2 MBP-SA3GCS was collected on the BioSAXS beamline (ID7A1) at the Cornell High Energy Synchrotron Source (CHESS) using a Superdex 200 10/300 GL column (GE Healthcare). Fe(II)-O2 MBP-SA3GCS samples were prepared in a buffer consisting of 50 mM Tris, 50 mM NaCl, 1 mM DTT, and 5% glycerol ( $\nu/\nu$ ) at pH 8.0. The sample was centrifuged at 30 psi for 20 min on a tabletop ultracentrifuge. A 100 µL volume at a concentration of 25 µM protein was loaded onto the SEC column and injected. SAXS data was collected sequentially with 2 s exposures with a flow rate of 0.5 mL min<sup>-1</sup>. Synchrotron beam was centered on a capillary sample cell with 1.5 mm path length and 25 µm thick quartzglass walls (Charles Supper Company, Natik, MA). The sample cell and full X-ray flight path, including beam stop, were kept in vacuo ( $< 1 \times 10^{-3}$  Torr) to eliminate air scatter. Temperature was maintained at 4 °C. Data were collected at 293 K using a dual PILATUS 100 K-S SAXS/WAXS detector and a wavelength of 1.264 Å. The sample capillary-to-detector distance was 1508.0 mm and was calibrated using silver behenate powder (The Gem Dugout, State College, PA). The useful q-space range  $(4\pi \text{Sin}\theta/\lambda \text{ with } 2\theta \text{ being the }$ scattering angle) was generally from qmin = 0.008 Å-1 to qmax = 0.27Å-1 ( $q = 4\pi \sin(\theta)/\lambda$ , where 20 is the scattering angle). The energy of the X-ray beam was 9.808 keV, with a flux of  $3 \times 10^{11}$  photons/s and a diameter of 250  $\mu m~\times~250~\mu m.$  The synchrotron storage ring was running at 50 milliamps positron current. Details of the SAXS data collection and model parameters are listed in Table S2.

The BioXTAS RAW software was used for SEC data collection, data reduction and background buffer data subtraction [33]. SAXS data were carefully chosen for averaging from frames that had the same radius of gyration across the dimer peak as from the UV plot of the SEC flowthrough (Fig. S5). Image integration, normalization, and subtraction was carried out using the RAW program. Radiation damage was assessed using the CORMAP criterion as implemented in RAW's built-in averaging function. Sample and buffer solutions were normalized to equivalent exposure before subtraction using beam-stop photodiode counts. The forward scattering I(0) and the radius of gyration  $(R_g)$  were calculated using the Guinier approximation, which assumes that at very small angles  $(q < 1.3/R_g)$  the intensity is approximated as  $I(q) = I(0)\exp[-1/R_g]$ 3(qRg) [2]]. The molecular mass was estimated using a comparison with glucose isomerase and lysozyme standard protein data in the RAW software. Guinear analysis and Kratky plots from the ATSAS program suite were performed to calculate the radius of gyration  $(R_{\sigma})$ , scattering intensity extrapolated to zero angle I(0), maximum dimension  $D_{max}$  and pair distance distribution P(r) (Fig. S6). GNOM [34] was used to calculate P(r), from which the Dmax and Rg were determined (Table S2). Ab initio low-resolution solution models were reconstructed using DAMMIN [35] for data in the range (0.012  $< q < 0.4 \text{ Å}^{-1}$ ) and with no symmetry. Ten models were generated from each program and averaged using DAMAVER [36]. The normalized spatial discrepancy parameter (NSD) obtained from DAMAVER indicated the similarity

between models used for average calculations. NSD values  $\leq 1.0$  were obtained as expected for similar models. The theoretical scattering profiles of the constructed models were calculated and fitted to experimental scattering data using CRYSOL. [37]

Individual domains of the MBP-SA3GCS protein with the MBP, globin, middle-domain and cyclase sequences and the dimer structures of the globin and cyclase domains were generated using homology modeling in the Swissmodel software. The models were scrutinized and validated by checking against high resolution protein structures of diguanylate cyclase and globin domain [38-42]. Possible tertiary and quaternary structures of MBP-SA3GCS were built manually into the SAXS solution envelope using the Pymol graphics software [43]. The overall dimer model was generated using the high scoring individual domain homology models of the MBP monomer, globin dimer, mid domain monomer and diguanylate cyclase dimer and merged. The fit of these sub-structures into the SAXS solution envelope was unambiguous due to the distinct features of the large MBP domains and the differences in the many domain and dimer sizes. The complete MBP-SA3GCS dimer model hence built was energy minimized using the Chimera [44] software. To evaluate the conformational flexibility of the individual domains in the manually fit dimer, SREFLEX [3] software was used with the domains and dimers refined as independent rigid bodies. This ATSAS program uses normal mode analysis to estimate the flexibility of highresolution models and improves their agreement with experimental SAXS data. The theoretical scattering was calculated for each generated model by CRYSOL. The Chi [2] fit for the MBP-SA3GCS dimer generated for the wild type and variants was close to 1.0, supporting the robustness of the SAXS models.

#### 2.10. Shewanella putrefaciens ssp. ANA3 GCS deletion strain

An internal portion of the SANA3 GCS gene was amplified by PCR and cloned into suicide vector pKO2.0 [45] to generate a vector pKO: $\Delta$  SANA3GCS.  $\Delta$ SANA3GCS was transformed into donor strain  $\beta$ -2155  $\lambda$  pir [46] and confirmed by DNA sequencing. pKO: $\Delta$ SANA3GCS was transferred into SANA3 by conjugation and single colonies were selected on media containing gentamycin (15 µg mL $^{-1}$ ). Single colonies were confirmed by PCR with primers SANA3GCSDTF and SANA3GCSDTR (Table S3).

#### 2.11. Quantitative biofilm assay

Congo Red assays were conducted as previously described. [47] Individual colonies of Shewanella ANA-3 (SANA3) and SANA3 ΔGCS from LB-agar plates were inoculated into 5 mL LB and cultured overnight in 15-mL plastic culture tubes. The overnights were inoculated 1:40 into 7 mL of LB containing 0.0025% Congo Red and aliquoted in 1.6 mL tubes (sterile, polypropylene; 1 mL per tube). For aerobic analysis, triplicates of WT and  $\Delta$ GCS cultures had the lids left loose for gas exchange and were loosely covered in Saran Wrap to prevent contamination; samples for anaerobic analysis were placed within a glass box with a seal and an AnaeroPack (BD Biosciences) was added to yield an O2-free atmosphere. The cultures were incubated for 24 h at 30 °C with shaking at 100 rpm. For biofilm quantification, samples were centrifuged at 12000 g for 15 min and 200 µL of supernatant were transferred to a 96-well microplate (Corning Costar; sterile, non-treated, polystyrene). The absorbance at 500 nm was recorded using a microplate reader. For normalization to cell growth, each culture was resuspended by pipetting and 200 µL were transferred to a 96-well microplate prior to recording the OD<sub>600</sub> using a microplate reader.

# 3. Results and discussion

# 3.1. SA3GCS binds heme and gaseous ligands

Shewanella sp. ANA-3 (SANA3) encodes a putative globin coupled

sensor protein (GCS; Shewana3\_0022, A0KR48; Fig. 1) that is composed of a N-terminal globin domain linked to a C-terminal GGDEF diguany-late cyclase domain. As heterologous expression of SA3GCS yielded red protein with characteristic Fe(II)-O<sub>2</sub> heme absorption spectrum, the ability of SA3GCS to bind gaseous ligands at the heme was probed by UV–visible absorption spectroscopy. SA3GCS Fe(II) has a Soret band  $\lambda_{\text{max}}$  at 425 nm and can bind O<sub>2</sub>, CO, and NO, resulting in blue shifts to 414, 419, and 416 nm, respectively (Fig. 2). The Q-band regions show the expected for each of the ferrous ligation states and the spectra in the various ligation states are similar to previously described GCS proteins [17,48], demonstrating that SA3GCS contains a functional sensor globin domain.

To further investigate  $O_2$  binding to SA3GCS, the  $O_2$  dissociation rate constants were measured using stopped-flow UV–vis spectroscopy (Fig. S1, Table 1). The measured progress curves are biphasic, described by two rate constants ( $k_1 = 1.96 \, \text{s}^{-1}$ ;  $k_2 = 73.4 \, \text{s}^{-1}$ , suggesting that there are at least two conformations of the heme pocket involved in sensing  $O_2$  [38,49–51]. SA3GCS remains in the Fe(II)- $O_2$  state while the protein is in an aerobic environment and oxidation of the Fe(II)- $O_2$  state to Fe(III) is not observed over the course of multiple hours of analysis. GCS proteins typically have very fast  $O_2$  association rates; the association rate constants for the GCS proteins from *B. pertussis* and *P. carotovorum* are  $\sim$ 7  $\mu$ M $^{-1}$  s $^{-1}$  [17]. Rapid  $O_2$  association generally results in  $K_D$ s for  $O_2$  in the mid-nM to low  $\mu$ M range, resulting in the proteins being fully  $O_2$  bound under aerobic conditions.

In comparison to BpeGReg and PccGCS, SA3GCS exhibits faster dissociation rate constants, especially for  $k_2$ . The GCS protein HemAT-Bs, which contains a methyl accepting chemotaxis protein output domain, has fast O<sub>2</sub> dissociation rate constants ( $k_1 = 87 \text{ s}^{-1}$  and  $k_2 =$ 1900 s<sup>-1</sup>), proposed to arise from an apolar distal pocket [51]. However, recent studies on the bifunctional GCS DcpG, which contains DGC and cdi-GMP phosphodiesterase output domains, found that the protein also exhibits fast O2 dissociation and that O2 dissociation rate constants are dependent on a heme edge histidine, with no other obvious differences in the heme pocket [52,53]. Both HemAT-Bs and DcpG contain a heme edge histidine and have at least one  $O_2$  dissociation rate  $> 70 \text{ s}^{-1}$ , while BpeGReg and PccGCS contain a heme edge tryptophan and have maximal O<sub>2</sub> dissociation rate constants <10 s<sup>-1</sup>. In contrast, SA3GCS contains a heme-edge tyrosine at the homologous position but otherwise similar heme pocket, suggesting that the heme edge position strongly regulates affinity for O2. The heme edge residue in DcpG was previously mutated, the H- > Y variant resulting in  $\sim$ 4-fold lower  $k_2$ , the H- > W variant resulting in  $\sim$ 17-fold decrease in  $k_2$ , and the H- > F variant resulting in  $\sim$ 44-fold decrease in  $k_2$  O<sub>2</sub> dissociation rate constants [53]. These data suggest that O2 dissociation rate constants are modulated by the hydrogen bonding capacity, hydrogen bond strength, and pKa of the heme edge residue, potentially by modulating electronic properties of the heme.

#### 3.2. Oxygen activates SA3GCS diguanylate cyclase activity

As previously characterized GCSs exhibit different diguanylate cyclase kinetics based on heme ligation state, SA3GCS diguanylate cyclase activity in response to different ligation states of the heme in the globin was determined. Initial studies compared the activity of Fe(II)-O<sub>2</sub> MBP-SA3GCS and SA3GCS constructs to determine if the MBP tag interfered with enzyme activity. MBP-SA3GCS was found to have a  $k_{cat}$  of  $1.88\pm0.054~\text{min}^{-1}$  and a  $K_{M}$  of  $32\pm4~\mu\text{M}$ ; in comparison, SA3GCS had a  $k_{cat}$  of  $3.05\pm0.11~\text{min}^{-1}$  and  $K_{M}$  of  $62\pm15~\mu\text{M}$  (Table 2). As the removal of the MBP tag from SA3GCS resulted in  $\sim$ 1.5-fold larger  $\nu_{max}$  under the same conditions, further enzymatic assays were performed on the MBP-cleaved SA3GCS construct.

Similar to previous work on *Bpe*GReg and *Pcc*GCS [16,17,23,48], cyclase activity of *SA*3GCS was the lowest for the Fe(II) unligated state (22% of maximum  $k_{\text{cat}}$ ) and highest for the Fe(II)-O<sub>2</sub> ligation state (100% of maximum  $k_{\text{cat}}$ ; Table 3). *SA*3GCS cyclase activity increased

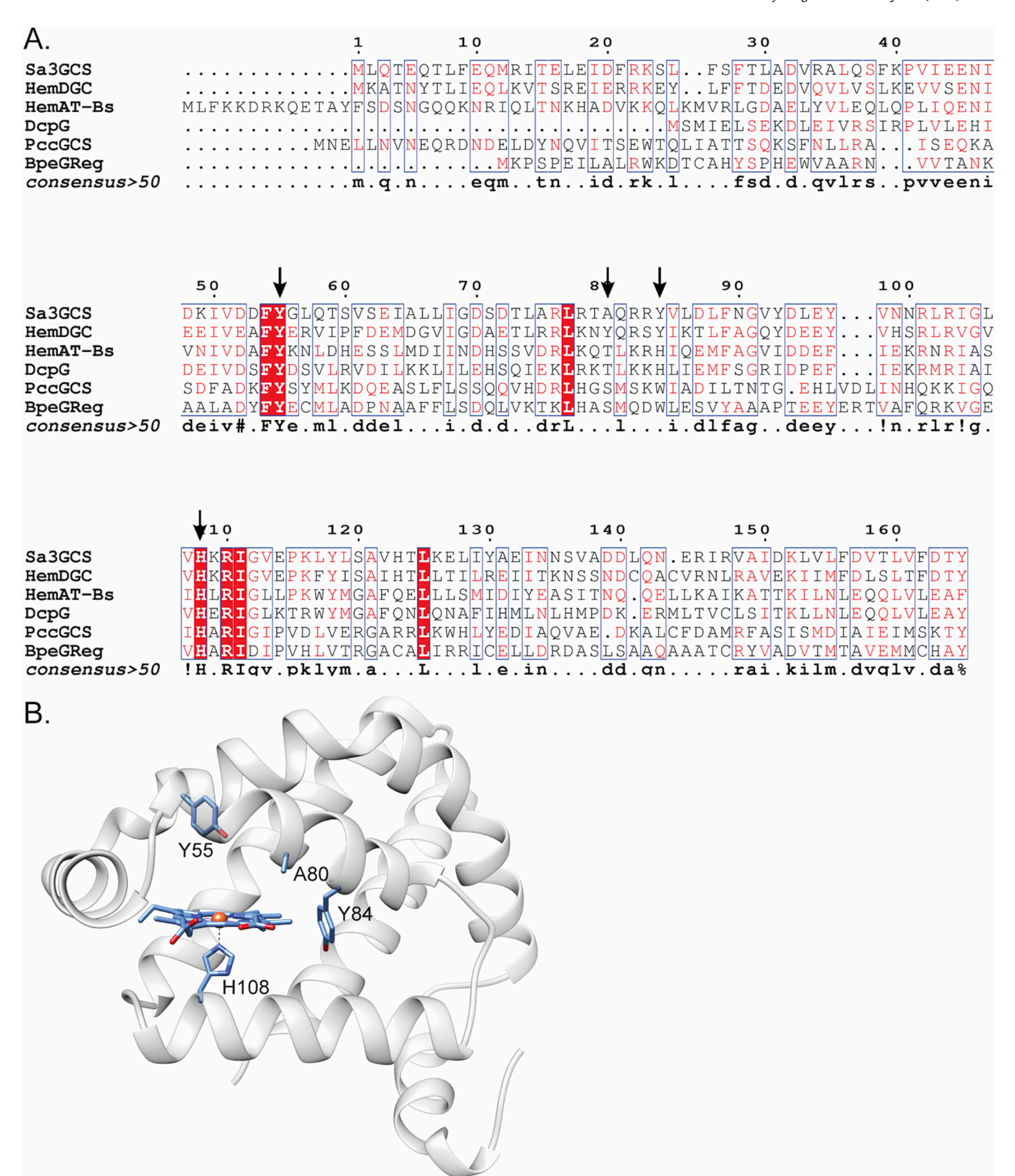
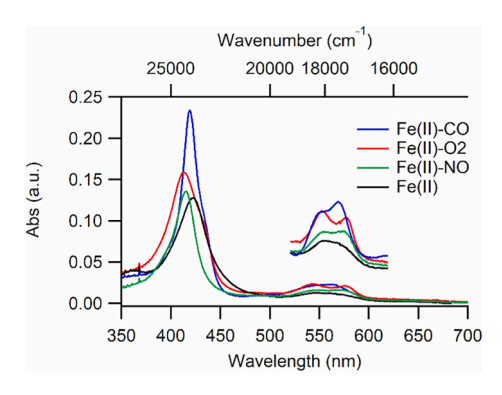


Fig. 1. SA3GCS sensor globin sequence alignment (A.) and homology model (B.). Residues discussed in the text are highlighted by arrows in A. and side chains shown in B.



**Fig. 2.** UV–visible spectra of SA3GCS Fe(II) unligated and ligated species. Black, Fe(II) (424, 550 nm); red, Fe(II) –  $O_2$  (414, 544, 577 nm); blue, Fe(II) – CO (419, 537, 565 nm); green, Fe(II) – NO (416, 543, 572 nm). The inset shows an expanded view of the Q-band region for clarity. (For interpretation of the references to colour in this figure legend, the reader is referred to the web version of this article.)

**Table 1** Rate constants for  $O_2$  dissociation from GCS proteins.  $\%k_1$  and  $k_2$  refer to the percentage of total amplitude due to each dissociation rate constant.

Protein	$k_1 (s^{-1})$	$k_2  (s^{-1})$	$\% k_1$	% k <sub>2</sub>	
SA3GCS	$1.96\pm0.06$	$\textbf{73.4} \pm \textbf{1.04}$	21.4	78.6	
PccGCS [17]	$0.641\pm0.003$	$3.98\pm0.03$	56.3	43.7	
BpeGReg [17]	$1.23\pm0.01$	$7.50\pm0.06$	36.2	63.8	
DcpG [53]	12.07	87.3	17.8	82.2	
HemAT-Bs [51]	87	1900	N.D.	N.D.	
EcDosC [23]	13	-	-	-	

N.D. Not determined.

**Table 2**Ligation state-dependent enzyme kinetics.

Protein	Ligation state	$k_{ m cat} \ ({ m min}^{-1})$	<i>K</i> <sub>M</sub> (μM)	$k_{\mathrm{cat}}/K_{\mathrm{M}}~(\mathrm{M}^{-1}\ \mathrm{min}^{-1})$
SA3GCS	Fe(II)	$0.67 \pm 0.08$	$60\pm12$	$11,167 \pm 2601$
	$Fe(II) - O_2$	$3.05\pm0.11$	$59\pm11$	$51,695 \pm 9817$
	Fe(II) - CO	$0.65\pm0.05$	$82\pm15$	$7927\pm1573$
	Fe(II) - NO	$0.83 \pm 0.08$	$74\pm20$	$11,\!216 \pm 3218$
BpeGReg [13]				
	Fe(II)	0.18	$120\ \pm$ $11$	1500
	$Fe(II) - O_2$	0.59	$57\pm8$	10,350
	Fe(II) - CO	0.23	ND	-
	Fe(II) - NO	0.38	ND	-
PccGCS [13]				
	Fe(II)	0.29	$62\pm3$	4677
	$Fe(II) - O_2$	0.73	$31\pm 6$	23,548
	Fe(II) - CO	0.43	N.D.	-
	Fe(II) - NO	0.51	N.D.	-

N.D. Not determined.

Table 3 GCS diguanylate cyclase percent relative activities based on initial rates of c-di-GMP product or  $k_{\rm cat}$ .

Protein	Fe(II)	Fe(II)-O <sub>2</sub>	Fe(II)-NO	Fe(II)-CO	Fe(III)
SA3GCS	22	100	27	21	N.D.
BpeGReg [17]	31	100	64	39	N.D.
PccGCS [17]	40	100	70	59	N.D.
EcDosC [23]	1.5	33	1.5	33	100
HemDGC [16]	0.9	100	0	0.6	0

N.D. Not determined.

only slightly in the Fe(II)-NO ligation state (27% of maximum  $k_{cat}$ ) and the Fe(II)-CO state did not cause significant changes in cyclase activity (21% of maximum  $k_{cat}$ ). These results suggest that SA3GCS is selective for O2 compared to other gaseous ligands. In comparison to other DGC containing GCS proteins, SA3GCS exhibited faster cyclization kinetics in the Fe(II)-O2 ligation state (Tables 2 and 3); SA3GCS was approximately 5-fold and 4-fold greater than GCS proteins with larger middle domains BpeGReg [17] and PccGCS [17], respectively. HemDGC, which also has a shorter middle domain and a heme edge tyrosine (Fig. 2), has maximum cyclase activity in the Fe(II)-O $_2$  (100% activity) and < 1% activity in the Fe(II)-unligated, Fe(II)-CO state, and Fe(II)-NO states (Table 3) [16]. In contrast, BpeGReg and PccGCS, which both contain longer middle domains and heme edge tryptophan residues, exhibit ~40% and 70% maximal activity in the Fe(II)-CO and Fe(II)-NO states, respectively. These results suggest that GCS proteins with a shorter middle domain and heme edge tyrosine exhibit greater ligand selectivity for the Fe(II)-O2 state to increase diguanylate cyclase activity. SA3GCS also does not exhibit ligation state-dependent differences in K<sub>M</sub>, as compared to PccGCS and BpeGReg, which exhibit 2–3-fold changes in  $K_{\rm M}$  between Fe (II) and Fe(II)-O2 states. Although Michaelis-Menten parameters were not calculated for HemDGC, results from SA3GCS studies suggest that the middle domain length of GCSs, and potentially the identity of the heme edge residue, modulate O2-dependent rearrangements of the catalytic domains that result in improved catalytic turnover of the diguanylate cyclase without significant rearrangement of the GTP binding

#### 3.3. Structural insights into SA3GCS

To investigate the  $\rm O_2$ -dependent activation, the oligomeric states of MBP-SA3GCS and SA3GCS constructs were determined in the Fe(II)- $\rm O_2$  ligation state by analytical gel filtration HPLC. SA3GCS and MBP-SA3GCS were predominantly a single oligomeric state, with calculated molecular weights of 156 (monomer, 46.7 kDa) and 353 kDa (monomer, 93 kDa), respectively. The SA3GCS oligomeric state is calculated as being either a tetrameric or trimeric state, likely due to an elongated conformation, while the MBP-SA3GCS was primarily tetrameric, regardless of concentration (Fig. 3, S7). However, the blue native gel of MBP-SA3GCS suggests that a small percentage of MBP-SA3GCS exists in the dimeric state (Fig. S8). These data suggest that both constructs form larger oligomeric states, as seen with several other GCS proteins [16,17,50].

Secondary structure changes were monitored to probe the effect of O2-dependent activation on MBP-SA3GCS. The Fe(II) ligation state of MBP-SA3GCS contained 77  $\pm$  10% helices, 5  $\pm$  1% turns, and 18  $\pm$  4% others (bend, loop; Fig. S3). Upon the addition of O2, the secondary structure changed to 58  $\pm$  7% helices, 5  $\pm$  1%  $\beta$ -strand, 7  $\pm$  2% turn, and 30  $\pm$  5% other. The changes in the secondary structure between the Fe(II) and Fe(II)-O2 ligation states suggest that O2 binding causes conformation changes to the enzyme that result in a decrease in the

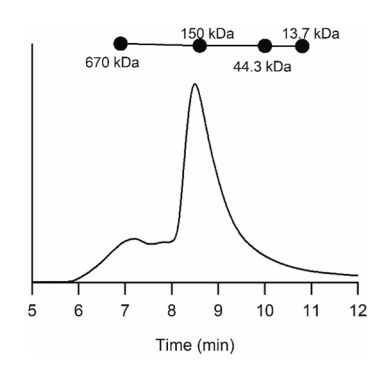


**Fig. 3.** Analytical gel filtration chromatogram of *SA*3GCS. The major peak ( $\sim$ 150 kDa) corresponds to a tetramer of *SA*3GCS.

helical content and an increase in the beta strand and random loop structures, as well as increased cyclase activity. The globin and cyclase domains individually are well folded as seen in the many homologous crystal structures [38–40]. Therefore, it is likely that these domains stay folded in the Fe(II) and Fe(II)-O<sub>2</sub> forms of the protein and the secondary structural changes seen in the CD experiment correlate to the changes in the middle domain. These data suggest that O<sub>2</sub> binding within the globin domain could result in a structural transition in the middle domain where helices unwind and allow for increased cyclase function.

To obtain further structural information about SA3GCS, DLS and SAXS were performed on Fe(II)-O<sub>2</sub> MBP-SA3GCS. The MBP-tagged protein was studied to ensure that 1) SA3GCS remained soluble and stable during the relatively long analysis times and 2) gain insight about mechanisms to decrease GCS diguanylate cyclase activity. The  $\sim$ 1.5-fold lower activity of MBP-SA3GCS vs. SA3GCS provided an opportunity to identify protein conformational changes involved in modulating GCS diguanylate cyclase activity. As characterized GCS proteins (Table 3) often exhibit only  $\sim$ 2.5–3-fold differences in cyclase activity between the "on" and "off" states of the enzymes, the difference in cyclase activity of MBP-SA3GCS and SA3GCS suggested that the MBP tag was potentially able to similarly alter GCS conformation to modulate catalytic activity without changing the ligation state of the heme iron.

Large aggregates (>100 nm) appeared in the size distribution of intensity in a DLS run of MBP-SA3GCS. Additionally, there appeared to be higher order oligomeric states present indicating the redistribution of oligomers after purification and over time. Therefore, inline-SEC was used for SAXS data collection of Fe(II)-O<sub>2</sub> MBP-SA3GCS run to remove any higher oligomers and protein aggregation that may have occurred with sample storage and travel to the synchrotron. Based on the peak intensities in the SEC trace (Fig. S5), we chose to focus on analysis of the dimer structure.

Due to a low starting concentration and five-fold dilution after the size exclusion column, the SEC-SAXS scattering signal was found to be weak, limited to a q-range of between 0 and 0.15 Å-1 as shown in Fig. S6. However, this was not limiting for further analysis and was found to be sufficient for low resolution structural information. The radius of gyration calculated through Guinear analysis was determined to be 51.05 Å and corresponded to that of a dimer, as expected. Based on the scattering intensity extrapolated to zero angle I(0), the molecular weight was calculated to be 230  $\pm$  50 kDa, supporting a dimeric state of MBP-SA3GCS (93 kDa). A solvent envelope reconstruction of MBP-SA3GCS, generated using the SAXS data input into the DAMMIN software, confirmed the dimensions and fit to a dimer model. The overall dimer model was generated by fitting and merging high scoring homology models of the MBP monomer (two copies), globin dimer, mid domain monomer (two copies) and diguanylate cyclase dimer into the DAMMIN generated solvent envelope.

Analysis of the model suggests that the orientation of each monomer of MBP-SA3GCS causes the observed lower cyclase activity, as compared to SA3GCS. It has been previously shown that DGC proteins require dimer formation for catalytic activity, with the active sites of each monomer facing each other and binding to one GTP molecule each and the cyclization reaction occurring across the dimer interface [41,42,54–56], regardless of their regulatory domain. The initial cyclase dimer modeled in SAXS was in its closed active-form with the two diguanylate cyclase active site halves proximal to each other, a requirement for enzymatic activity for the conversion of GTP to c-di-GMP. However, after refinement with SREFLEX (improvement of correlation coefficient from 0.94 to 0.99), the two monomers of the cyclase moved apart and formed an open structure with altered orientation of the two cyclase domains within the SAXS envelope that did not position the active sites at an optimal distance. The distance between cyclase domain active sites should result in lower enzymatic activity, as was observed for MPB-SA3GCS compared to SA3GCS (Table 1), suggesting that hinging of the diguanylate cyclase domains could serve as a mechanism to regulate enzymatic activity while maintaining the dimer

through globin domain interactions. This movement of diguanylate cyclase domains regulating enzyme activity is similar to those observed for DcpG, which contains both diguanylate cyclase and phosphodiesterase output domains [53], and may be a conserved method of enzymatic regulation in GCS proteins.

In agreement with the CD data, the middle domain homology model was modeled as a helix-turn-helix in the open inactive state and a flexible unstructured loop in the open active state. The middle domain hence could help in the reorientation of the diguanylate cyclase monomers as it changes from open to closed states. A model of the potential active cyclase conformation was developed (Fig. 4C), highlighting possible domain movements. The protein quaternary structure could be controlled by the crucial middle-domain as it transitions between two related dimeric states, inactive (open) and active (closed) (Fig. 4A and B; and 4C, respectively). In addition, the cyclase could also transition between the open-closed states upon substrate binding to the active site.

# 3.4. GCS impacts biofilm formation of Shewanella ssp. ANA3

As c-di-GMP produced by diguanylate cyclases has been shown to regulate biofilm formation [57], the function of the globin-coupled sensor was elucidated by deleting the GCS from SANA3 ( $\Delta GCS$ ). The biofilm formation of both the wild-type and the deletion strains were monitored under aerobic and anaerobic conditions. Under both conditions, SANA3 \(\Delta GCS\) exhibited decreased biofilm formation, as compared to WT SANA3 (Fig. 5). While diguanylate cyclase activity, which results in c-di-GMP production, is typically linked with increasing biofilm formation, recent work has demonstrated that diguanylate cyclases can control many additional cellular phenotypes [10,25]. Shewanella sp. ANA-3 encodes for 60 proteins predicted to contain diguanylate cyclase (GGDEF) domains, although some of the domains may be catalytically inactive, suggesting that c-di-GMP signaling likely controls many other cellular pathways and phenotypes, in addition to biofilm formation. Furthermore, the increased biofilm formation observed under anaerobic conditions is likely controlled by an a different diguanylate cyclase, as the SANA3  $\triangle GCS$  strain is still exhibits O<sub>2</sub>-dependent biofilm formation. However, as the relative increase in biofilm formation under anaerobic vs. aerobic conditions is slightly attenuated in the SANA3  $\Delta GCS$  strain (6.7-fold for WT and 5.5-fold for  $\Delta GCS$ ), SA3GCS may be involved in regulating additional cellular processes involved in adapting to environments with different O2 concentrations. Overall, these results demonstrate that SA3GCS is active in vivo and affects Shewanella sp. ANA3 biofilm formation, as well as suggest that SA3GCS may be involved in regulating other c-di-GMP-dependent pathways in response to O<sub>2</sub> levels, such as metabolism, growth, or motility.

#### 4. Conclusion

In summary, the results have demonstrated that SA3GCS serves as a globin coupled sensor that exhibits ligand-dependent diguanylate cyclase activity and plays a role in biofilm formation of Shewanella sp. ANA3 in vivo. Using SAXS, we have developed a model of MBP-SA3GCS and identified possible rearrangements involved in ligand-dependent regulation of cyclase activity. Based on CD and SAXS data, the middle domain is involved with the conformational changes required for signal transduction from the globin to the cyclase domain, allowing for conversion between inactive and active forms of the enzyme. Furthermore, the heme edge tyrosine may be involved in transmitting the heme ligand identity through the protein to regulate enzyme activity. This work suggests a potential mechanism for O2-dependent conformational changes in regulating GCS protein activity by changing cyclase domain orientation and in modulating bacterial biofilm formation.

# Author statement

Ariel Schuelke-Sanchez: Conceptualization, methodology,

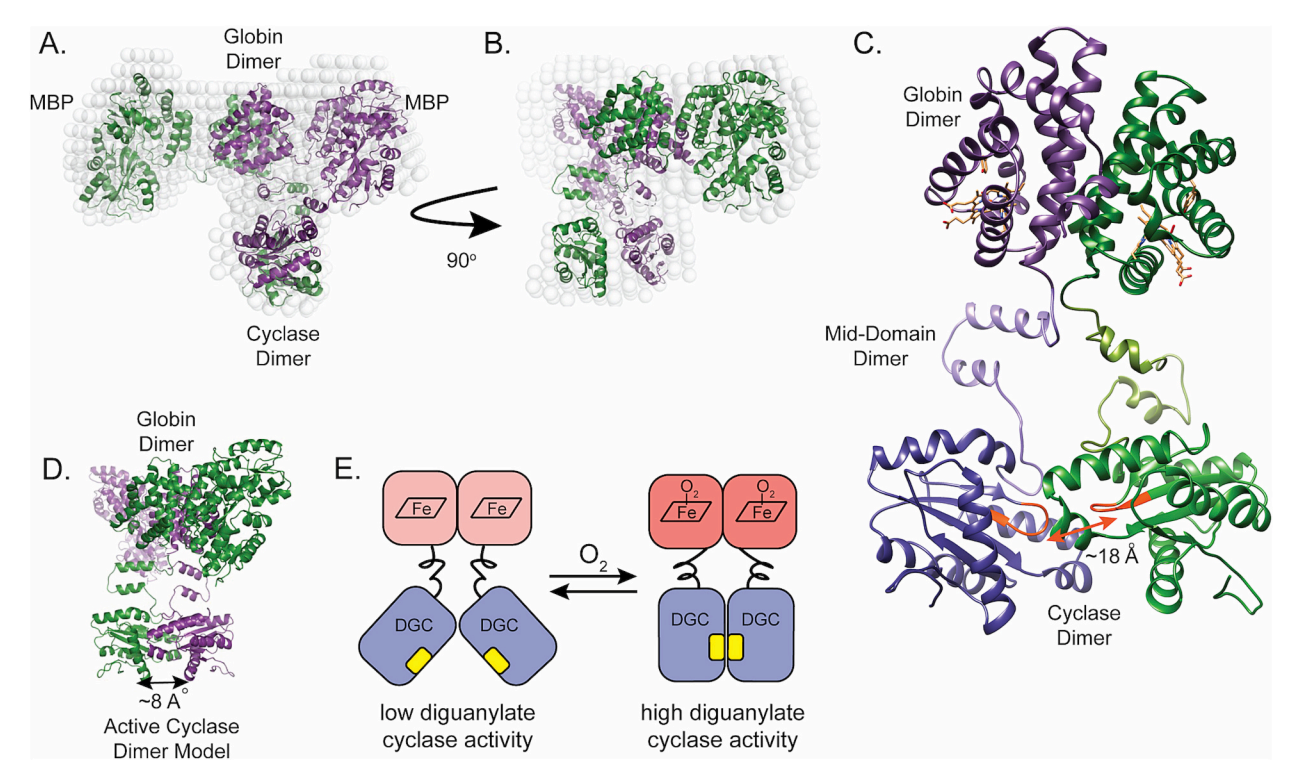


Fig. 4. SA3GCS SAXS model. A.) Dammin generated bead model (in grey) superimposed with the MBP-SA3GCS dimer model cartoon and B.) a 90° rotated view of the MBP-SA3GCS dimer model. The dimer model was generated using the modeling software Swissmodel. [1] C.) Final SAXS model of SA3GCS dimer, omitting the MBP domains. Monomer colors (green, purple) vary by domain. The diguanylate cyclase domain active sites (GGDEF) are highlighted in orange and are ~18 Å apart. High scoring individual domain models were generated for the globin dimer, mid domain and diguanylate cyclase dimer and merged as shown in D.) as a closed active site dimer (active sites ~8 Å apart). When this merged model was refined against the SAXS data using normal mode analysis in the ATSAS [2] suite SREFLEX [3], the diguanylate cyclase dimer moved apart from each other to form an inactive/open dimer shown as black arrows. E.) Model for regulation of diguanylate cyclase activity based on the SAXS data. (For interpretation of the references to colour in this figure legend, the reader is referred to the web version of this article.)

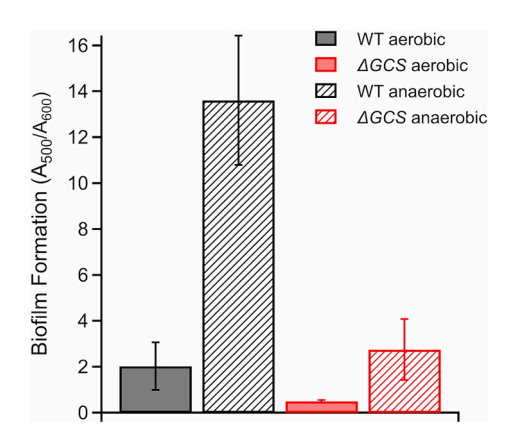


Fig. 5. Biofilm quantification of *Shewanella* sp. ANA3 WT (black) and  $\Delta$ GCS (red) under aerobic (solid) and anaerobic (striped) conditions. (For interpretation of the references to colour in this figure legend, the reader is referred to the web version of this article.)

investigation, analysis, validation, writing.; Neela Yennawar: investigation, analysis.; Emily Weinert: conceptualization, methodology, investigation, writing, supervision, funding acquisition.

#### CRediT authorship contribution statement

**Ariel Schuelke-Sanchez:** Writing – original draft, Methodology, Investigation, Formal analysis. **Neela H. Yennawar:** Writing – original draft, Methodology, Investigation. **Emily E. Weinert:** Writing – review & editing, Writing – original draft, Supervision, Project administration,

Methodology, Investigation, Funding acquisition, Formal analysis, Conceptualization.

# Declaration of competing interest

The authors declare that they have no known competing financial interests or personal relationships that could have appeared to influence the work reported in this paper.

#### Data availability

Data will be made available on request.

# Acknowledgements

This work was supported by NSF grants CHE1352040 (E.E.W.), CHE2003350 (E.E.W.), and CHE2312149 (E.E.W.) and Frasch Foundation grant 824-H17 (E.E.W.). These studies are based upon research conducted at the Cornell High Energy Synchrotron Source (CHESS). We would like to acknowledge staff scientist Dr. Richard Gillilan for enabling SAXS data collection. CHESS is supported by the NSF & NIH/NIGMS via NSF award DMR-1829070, and the MacCHESS resource is supported by NIH/NIGMS award GM-124166. The authors thank Julia Fecko for the assistance with the circular dichroism spectroscopy data and the Huck Institutes of the Life Sciences at The Pennsylvania State University for the continued support of the Penn State Automated Biological Calorimetry and Crystallography Facility and Dr. Justin Burns for his help with generation of the SANA3  $\Delta GCS$  strain.

#### Appendix A. Supplementary data

Supplementary data to this article can be found online at https://doi.org/10.1016/j.jinorgbio.2024.112482.

#### References

- [1] A. Waterhouse, M. Bertoni, S. Bienert, G. Studer, G. Tauriello, R. Gumienny, F. T. Heer, T.A.P. de Beer, C. Rempfer, L. Bordoli, R. Lepore, T. Schwede, SWISS-MODEL: homology modelling of protein structures and complexes, Nucleic Acids Res. 46 (2018) W296–W303.
- [2] D. Franke, M.V. Petoukhov, P.V. Konarev, A. Panjkovich, A. Tuukkanen, H.D. T. Mertens, A.G. Kikhney, N.R. Hajizadeh, J.M. Franklin, C.M. Jeffries, D. I. Svergun, ATSAS 2.8: a comprehensive data analysis suite for small-angle scattering from macromolecular solutions, J. Appl. Crystallogr. 50 (2017) 1212-1225
- [3] A. Panjkovich, D.I. Svergun, Deciphering conformational transitions of proteins by small angle X-ray scattering and normal mode analysis, Phys. Chem. Chem. Phys. 18 (2016) 5707–5719
- [4] H.H. Hau, J.A. Gralnick, Ecology and biotechnology of the genus Shewanella, Annu. Rev. Microbiol. 61 (2007) 237–258.
- [5] J.M. Tiedje, Shewanella—the environmentally versatile genome, Nat. Biotechnol. 20 (2002) 1093–1094.
- [6] J.F. Heidelberg, I.T. Paulsen, K.E. Nelson, E.J. Gaidos, W.C. Nelson, T.D. Read, J. A. Eisen, R. Seshadri, N. Ward, B. Methe, R.A. Clayton, T. Meyer, A. Tsapin, J. Scott, M. Beanan, L. Brinkac, S. Daugherty, R.T. DeBoy, R.J. Dodson, A.S. Durkin, D.H. Haft, J.F. Kolonay, R. Madupu, J.D. Peterson, L.A. Umayam, O. White, A. M. Wolf, J. Vamathevan, J. Weidman, M. Impraim, K. Lee, K. Berry, C. Lee, J. Mueller, H. Khouri, J. Gill, T.R. Utterback, L.A. McDonald, T.V. Feldblyum, H. O. Smith, J.C. Venter, K.H. Nealson, C.M. Fraser, Genome sequence of the dissimilatory metal ion–reducing bacterium Shewanella oneidensis, Nat. Biotechnol. 20 (2002) 1118–1123.
- [7] G.M. Barbara, J.G. Mitchell, Bacterial tracking of motile algae, FEMS Microbiol. Ecol. 44 (2003) 79–87.
- [8] M. Zhang, B.R. Ginn, T.J. DiChristina, A.G. Stack, Adhesion of Shewanella oneidensis MR-1 to Iron (oxy)(Hydr)oxides: microcolony formation and isotherm, Environ. Sci. Technol. 44 (2010) 1602–1609.
- [9] R.M. Donlan, Biofilm formation: a clinically relevant microbiological process, Clin. Infect. Dis. 33 (2001) 1387–1392.
- [10] R. Hengge, Principles of c-di-GMP signalling in bacteria, Nat. Rev. Microbiol. 7 (2009) 263–273.
- [11] J.S. McLean, G.E. Pinchuk, O.V. Geydebrekht, C.L. Bilskis, B.A. Zakrajsek, E.A. Hill, D.A. Saffarini, M.F. Romine, Y.A. Gorby, J.K. Fredrickson, A.S. Beliaev, Oxygendependent autoaggregation in Shewanella oneidensis MR-1, Environ. Microbiol. 10 (2008) 1861–1876.
- [12] J.L. Burns, P.B. Jariwala, S. Rivera, B.M. Fontaine, L. Briggs, E.E. Weinert, Oxygen-dependent globin coupled sensor signaling modulates motility and virulence of the plant pathogen Pectobacterium carotovorum, ACS Chem. Biol. 12 (2017) 2070–2077.
- [13] H. Sass, M. Berchtold, J. Branke, H. König, H. Cypionka, H.-D. Babenzien, Psychrotolerant sulfate-reducing Bacteria from an Oxic freshwater sediment description of Desulfovibrio cuneatus sp. nov. and Desulfovibrio litoralis sp. nov, Syst. Appl. Microbiol. 21 (1998) 212–219.
- [14] J. Green, J.C. Crack, A.J. Thomson, N.E. LeBrun, Bacterial sensors of oxygen, Curr. Opin. Microbiol. 12 (2009) 145–151.
- [15] C. Wu, Y.Y. Cheng, H. Yin, X.N. Song, W.W. Li, X.X. Zhou, L.P. Zhao, L.J. Tian, J. C. Han, H.Q. Yu, Oxygen promotes biofilm formation of Shewanella putrefaciens CN32 through a diguanylate cyclase and an adhesin, Sci. Rep. 3 (2013) 1945–1951.
- [16] H. Sawai, S. Yoshioka, T. Uchida, M. Hyodo, Y. Hayakawa, K. Ishimori, S. Aono, Molecular oxygen regulates the enzymatic activity of a heme-containing diguanylate cyclase (HemDGC) for the synthesis of cyclic di-GMP, Biochim. Biophys. Acta 1804 (2010) 166–172.
- [17] J.L. Burns, D.D. Deer, E.E. Weinert, Oligomeric state affects oxygen dissociation and diguanylate cyclase activity of globin coupled sensors, Mol. BioSyst. 10 (2014) 2823–2826.
- [18] J.L. Burns, S. Rivera, D.D. Deer, S.C. Joynt, D. Dvorak, E.E. Weinert, Oxygen and c-di-GMP binding control oligomerization state equilibria of Diguanylate cyclase-containing globin coupled sensors, Biochemistry 55 (2016) 6642–6651.
- [19] J. Donné, M. Van Kerckhoven, L. Maes, P. Cos, S. Dewilde, The role of the globin-coupled sensor YddV in a mature E. Coli biofilm population, Biochim. Biophys. Acta 1864 (2016) 835–839.
- [20] S. Hou, C. Belisle, S. Lam, M. Piatibratov, V. Sivozhelezov, H. Takami, M. Alam, A globin-coupled oxygen sensor from the facultatively alkaliphilic bacillus halodurans C-125, Extremophiles 5 (2001) 351–354.
- [21] S. Hou, T. Freitas, R.W. Larsen, M. Piatibratov, V. Sivozhelezov, A. Yamamoto, E. A. Meleshkevitch, M. Zimmer, G.W. Ordal, M. Alam, Globin-coupled sensors: a class of heme-containing sensors in Archaea and Bacteria, Proc. Natl. Acad. Sci. U. S. A. 98 (2001) 9353–9358.
- [22] K. Kitanishi, K. Kobayashi, T. Uchida, K. Ishimori, J. Igarashi, T. Shimizu, Identification and functional and spectral characterization of a globin-coupled histidine kinase from Anaeromyxobacter sp. Fw109-5, J. Biol. Chem. 286 (2011) 35522–35534.
- [23] K. Kitanishi, K. Kobayashi, Y. Kawamura, I. Ishigami, T. Ogura, K. Nakajima, J. Igarashi, A. Tanaka, T. Shimizu, Important roles of Tyr43 at the putative heme

- distal side in the oxygen recognition and stability of the Fe(II)-O2 complex of YddV, a globin-coupled heme-based oxygen sensor diguanylate cyclase, Biochemistry 49 (2010) 10381–10393.
- [24] J.R. Tuckerman, G. Gonzalez, E.H. Sousa, X. Wan, J.A. Saito, M. Alam, M.A. Gilles-Gonzalez, An oxygen-sensing diguanylate cyclase and phosphodiesterase couple for c-di-GMP control, Biochemistry 48 (2009) 9764–9774.
- [25] U. Jenal, A. Reinders, C. Lori, Cyclic di-GMP: second messenger extraordinaire, Nat. Rev. Microbiol. 15 (2017) 271–284.
- [26] Johnnie A. Walker, Y. Wu, Jacob R. Potter, Emily E. Weinert, π-Helix controls activity of oxygen-sensing diguanylate cyclases, Biosci. Rep. 40 (2020).
- [27] E.E. Weinert, L. Plate, C.A. Whited, C. Olea Jr., M.A. Marletta, Determinants of ligand affinity and heme reactivity in H-NOX domains, Angew. Chem. Int. Ed. Eng. 49 (2010) 720–723.
- [28] E.M. Boon, S.H. Huang, M.A. Marletta, A molecular basis for NO selectivity in soluble guanylate cyclase, nature Chem, Biol. 1 (2005) 53–59.
- [29] D.S. Karow, D. Pan, R. Tran, P. Pellicena, A. Presley, R.A. Mathies, M.A. Marletta, Spectroscopic characterization of the soluble guanylate cyclase-like heme domains from vibrio cholerae and Thermoanaerobacter tengcongensis, Biochemistry 43 (2004) 10203–10211.
- [30] N.J. Hoque, M.P. Helm, E.E. Weinert, In vitro measurement of gas-dependent and redox-sensitive Diguanylate cyclase activity, Methods Mol. Biol. 2648 (2023) 75–86.
- [31] Y. Sasakura, S. Hirata, S. Sugiyama, S. Suzuki, S. Taguchi, M. Watanabe, T. Matsui, I. Sagami, T. Shimizu, Characterization of a direct oxygen sensor heme protein from Escherichia coli, Effects of the heme redox states and mutations at the heme-binding site on catalysis and structure, J. Biol. Chem. 277 (2002) 23827-23827.
- [32] A. Micsonai, F. Wien, L. Kernya, Y.-H. Lee, Y. Goto, M. Réfrégiers, J. Kardos, Accurate secondary structure prediction and fold recognition for circular dichroism spectroscopy, Proc. Natl. Acad. Sci. 112 (2015) E3095–E3103.
- [33] J.B. Hopkins, R.E. Gillilan, S. Skou, BioXTAS RAW: improvements to a free open-source program for small-angle X-ray scattering data reduction and analysis, J. Appl. Crystallogr. 50 (2017) 1545–1553.
- [34] D. Svergun, Determination of the regularization parameter in indirect-transform methods using perceptual criteria, J. Appl. Crystallogr. 25 (1992) 495–503.
- [35] D.I. Svergun, Restoring low resolution structure of biological macromolecules from solution scattering using simulated annealing, Biophys. J. 76 (1999) 2879–2886.
- [36] V.V. Volkov, D.I. Svergun, Uniqueness of ab initio shape determination in small-angle scattering, J. Appl. Crystallogr. 36 (2003) 860–864.
- [37] D. Svergun, C. Barberato, M.H.J. Koch, CRYSOL a program to evaluate X-ray solution scattering of biological macromolecules from atomic coordinates, J. Appl. Crystallogr. 28 (1995) 768–773.
- [38] S. Rivera, P.G. Young, E.D. Hoffer, G.E. Vansuch, C.L. Metzler, C.M. Dunham, E. E. Weinert, Structural insights into oxygen-dependent signal transduction within globin coupled sensors, Inorg. Chem. 57 (2018) 14386–14395.
- [39] M. Tarnawski, T.R. Barends, I. Schlichting, Structural analysis of an oxygen-regulated diguanylate cyclase, Acta Crystallogr. Sect. D: Biol. Crystallogr. 71 (2015) 2158–2177.
- [40] W. Zhang, G.N. Phillips, Structure of the oxygen sensor in Bacillus subtilis: signal transduction of chemotaxis by control of symmetry, Structure 11 (2003) 1097–1110.
- [41] P. Wassmann, C. Chan, R. Paul, A. Beck, H. Heerklotz, U. Jenal, T. Schirmer, Structure of BeF3--modified response regulator PleD: implications for diguanylate cyclase activation, catalysis, and feedback inhibition, Structure 15 (2007) 915–927.
- [42] A. Deepthi, C.W. Liew, Z.-X. Liang, K. Swaminathan, J. Lescar, Structure of a Diguanylate cyclase from Thermotoga maritima: insights into activation, feedback inhibition and Thermostability, PLoS One 9 (2014) e110912.
- [43] The PyMOL Molecular Graphics System, Version 1.2r3pre, Schrödinger, LLC.
- [44] E.F. Pettersen, T.D. Goddard, C.C. Huang, G.S. Couch, D.M. Greenblatt, E.C. Meng, T.E. Ferrin, UCSF chimera—a visualization system for exploratory research and analysis, J. Comput. Chem. 25 (2004) 1605–1612.
- [45] J.L. Burns, T.J. DiChristina, Anaerobic respiration of elemental sulfur and thiosulfate by Shewanella oneidensis MR-1 requires psrA, a homolog of the phsA gene of salmonella enterica serovar typhimurium LT2, Appl. Environ. Microbiol. 75 (2009) 5209–5217.
- [46] C. Dehio, M. Meyer, Maintenance of broad-host-range incompatibility group P and group Q plasmids and transposition of Tn5 in Bartonella henselae following conjugal plasmid transfer from Escherichia coli, J. Bacteriol. 179 (1997) 538–540.
- [47] A. Spiers, J. Bohannon, S. Gehrig, P. Rainey, Biofilm formation at the air-liquid interface by the *Pseudomonas fluorescens* SBW25 wrinkly spreader requires an acetylated form of cellulose, Mol. Microbiol. 50 (2003) 15–27.
- [48] X. Wan, J.R. Tuckerman, J.A. Saito, T.A. Freitas, J.S. Newhouse, J.R. Denery, M. Y. Galperin, G. Gonzalez, M.A. Gilles-Gonzalez, M. Alam, Globins synthesize the second messenger bis-(3'-5')-cyclic diguanosine monophosphate in bacteria, J. Mol. Biol. 388 (2009) 262–270.
- [49] T. Ohta, H. Yoshimura, S. Yoshioka, S. Aono, T. Kitagawa, Oxygen-sensing mechanism of HemAT from Bacillus subtilis: a resonance Raman spectroscopic study, J. Am. Chem. Soc. 126 (2004) 15000–15001.
- [50] S. Rivera, J.L. Burns, G.E. Vansuch, B. Chica, E.E. Weinert, Globin domain interactions control heme pocket conformation and oligomerization of globin coupled sensors, J. Inorg. Biochem. 164 (2016) 70–76.
- [51] W. Zhang, J.S. Olson, G.N. Phillips Jr., Biophysical and kinetic characterization of HemAT, an aerotaxis receptor from Bacillus subtilis, Biophys. J. 88 (2005) 2801–2814.

- [52] D.C. Patterson, M.P. Ruiz, H. Yoon, J.A. Walker, J.-P. Armache, N.H. Yennawar, E. E. Weinert, Differential ligand-selective control of opposing enzymatic activities within a bifunctional c-di-GMP enzyme, PNAS 118 (2021) e2100657118.
- [53] D.C. Patterson, Y. Liu, S. Das, N.H. Yennawar, J.P. Armache, J.R. Kincaid, E. E. Weinert, Heme-edge residues modulate signal transduction within a bifunctional Homo-dimeric sensor protein, Biochemistry 60 (2021) 3801–3812.
- [54] C. Chan, R. Paul, D. Samoray, N.C. Amiot, B. Giese, U. Jenal, T. Schirmer, Structural basis of activity and allosteric control of diguanylate cyclase, Proc. Natl. Acad. Sci. U. S. A. 101 (2004) 17084–17089.
- [55] N. De, M.V. Navarro, R.V. Raghavan, H. Sondermann, Determinants for the activation and autoinhibition of the diguanylate cyclase response regulator WspR, J. Mol. Biol. 393 (2009) 619–633.
- [56] R. Paul, S. Abel, P. Wassmann, A. Beck, H. Heerklotz, U. Jenal, Activation of the diguanylate cyclase PleD by phosphorylation-mediated dimerization, J. Biol. Chem. 282 (2007) 29170–29177.
- [57] U. Romling, Cyclic di-GMP signaling-where did you come from and where will you go? Molecular Microbiology 120 (2023) 564–574.